Available online at www.sciencedirect.com
SCIENCE DIRECT
Polymer 46 (2005) 11035–11050
polymer
www.elsevier.com/locate/polymer

Simulations of the mobile phase of polyethylene

T.L. Phillips, S. Hanna*

H. H. Wills Physics Department, University of Bristol, Tyndall Avenue, Bristol BS8 1TL, UK

Received 12 April 2005; received in revised form 4 September 2005; accepted 5 September 2005
Available online 4 October 2005

Abstract

Results are presented from atomistic molecular dynamics simulations of the mobile pseudo-hexagonal phase of polyethylene, which occurs under conditions of elevated pressure and temperature. Three different types of model are considered, all of which employ periodic boundary conditions. The first model consists of *n*-alkane sequences ($48\times$–$C_{24}H_{48}$–) that are bonded across the simulation box boundaries to produce chains that are effectively infinite in extent. On heating, at high pressure, this system displays a rotator phase, in which the chains retain an all-*trans* conformation, and rotate as semi-rigid units. A second model, consisting of finite *n*-alkanes ($48\times C_{24}H_{50}$) displays the same behaviour at low temperatures, but at high temperature and pressure forms a conformationally disordered rotator phase, characterised by a large proportion of *gauche* defects and a significant lattice expansion. The final model considered contains long *n*-alkanes ($24\times C_{102}H_{206}$) which contain jog defects and each pass twice through the simulation box. This model forms a conformationally disordered rotator phase at high temperature and ambient pressure. The behaviour of the three models, in terms of the variations in chain conformation and rotational and translational dynamics, are compared. The conformationally disordered phases provide useful representations of the experimentally observed mobile phase.

Keywords: Polyethylene; *n*-Alkanes; Computer simulation

1. Introduction

In this paper, we consider the structure and dynamics of the mobile phase of polyethylene. At ambient pressure and temperature, it is well known that polyethylene forms an orthorhombic crystal structure. On heating at high pressure, a phase transition occurs to a phase in which the polymer chains have a hexagonal packing arrangement [1–6]. The phase is often referred to as a pseudo-hexagonal phase, to emphasise the fact that, although the unit cell parameters correspond to a hexagonal crystal class, the unit cell motif is unlikely to conform to a precise hexagonal symmetry. It was observed that chain-folded crystals of polyethylene underwent rapid thickening parallel to the chain direction, when held in the pseudo-hexagonal phase, from which it was inferred that the polymer chains must be mobile, undergoing translational diffusion parallel to their length. Thus, the phase has become known as the 'mobile phase' of polyethylene. The requirement of hexagonal packing, led to the suggestion that the polymer chain-stems must be dynamically rotationally disordered in the mobile phase, and so the term 'rotator phase' was also adopted, although there was no direct evidence for chain rotation in the original X-ray analysis. The terms, 'mobile phase', 'rotator phase' and 'pseudo-hexagonal phase' tend to be used interchangeably in the literature when referring to the high pressure/high temperature phase of polyethylene.

The mobile phase has been characterised extensively by X-ray analysis [2–5], infrared spectroscopy [7,8] and NMR [9–11]. The picture that has emerged, is one of conformationally disordered chain-stems, which are rich in *gauche* defects, and which undergo frequent rotations parallel to the chain axes. The disorder is dynamic: the locations of *gauche* defects along the chains are constantly changing, and the chains are diffusing longitudinally.

The rapid thickening of the lamellae in the mobile phase of polyethylene has attracted much interest, both in producing oriented materials with enhanced mechanical properties [12,13] and as a possible mechanism involved in the initial formation of lamellar crystals [14]. Studies of the crystal growth at elevated pressures have indicated that even in a thickening growth regime, chains are initially deposited at the lamellar growth front in a folded form [15]. This has led to investigations into the mechanisms that determine the lamellar thickness and the possibility of an ambient-pressure size-dependent mobile-phase, i.e. a phase that would allow chains to slide rapidly when first deposited on the crystal growth face,

* Corresponding author. Tel.: +44 117 928 8771; fax: +44 117 925 5624.
E-mail address: s.hanna@bristol.ac.uk (S. Hanna).

0032-3861/$ - see front matter © 2005 Elsevier Ltd. All rights reserved.
doi:10.1016/j.polymer.2005.09.019

but would then transform to the orthorhombic phase on achieving a particular thickness.

Rotator phases are also observed in short *n*-alkane crystals, in which case the application of pressure is not necessary. Several phases of different symmetry have been identified, but the main difference between these phases and that observed in polyethylene, is that the *n*-alkane chains retain a *trans* conformation, and rotate as rigid or semi-rigid units.

A considerable number of computer investigations into the crystalline phases of polyethylene have appeared in the literature. The tendency has been to model comparatively short *n*-alkanes, up to around 50 carbon atoms in the backbone of each chain, and then to treat these as models for polyethylene. The main drawback to this approach is that no allowance is made for the presence of chain folds. For example, simulations of the orthorhombic phases of *n*-alkanes have been reported in Refs. [16–23]. An alternative approach, which is successful in modelling the orthorhombic phase of polyethylene, is to bond the *n*-alkane across the periodic boundaries of the simulation box, in order to generate infinitely long chains (see e.g. Refs. [21,23–25]). A number of simulations have been presented of the rotator phases of both finite and infinite alkane systems [26–29]. However, in all cases a conformationally ordered phase was simulated, consisting of rigid or near-rigid rotors.

The only attempts in the literature to model conformationally disordered chains are from Sumpter and co-workers [30], who have simulated systems of united-atom chains, i.e. chains in which the CH_2 units are treated as spheres, at high temperatures, and have observed the creation of *gauche* defects, g^+tg^- kinks (see below) and chain mobility. However, no attempt was made to apply high pressure to the simulations, and the use of united atoms is now recognised as biasing the crystal structures formed, and promoting enhanced chain mobility at all temperatures.

In this paper, we will consider three possible candidates for simulating the conformationally disordered phase of polyethylene at high pressure and temperature. Two of the models are traditional, in the sense that they consist of straight *n*-alkane segments, in both finite and infinite chain arrangements. The third model consists of a novel arrangement in which long *n*-alkane chains pass twice through the simulation box, with jog defects incorporated at the midpoint of each chain to prevent chain overlap. This model has previously been used to study the orthorhombic phase of polyethylene, and has the advantage that the jogs mimic the behaviour of chain-folds, and add an extra level of realism to the simulations [23]. The mobile phases present in each system will be explored, and their behaviours compared and contrasted.

2. Simulation methods

2.1. Choice of models

The selection of suitable models for simulating crystalline polyethylene has been discussed elsewhere [23]. The main difficulty in producing an accurate representation is due to the fact that real polyethylene crystals are inherently disordered, the disorder arising from several sources including the presence of chain ends and branches, and, at a more fundamental level, the finite size of the crystallites and the presence of chain folds. Ideally, a computer model should capture all of these effects, if it is to succeed in predicting the behaviour of real systems. The main barrier to building such a model is the fact that any realistic model must necessarily be very large, if it is to incorporate defects in the correct concentration.

A consequence of this consideration is that the realism of computer models for polyethylene crystals will be limited by the computational resources available, and it is inevitable, therefore, that our models will give only qualitative agreement with experimental behaviour. This is especially true in the present case, where we are interested in modelling mobile, pseudo-hexagonal phases, which include a significantly larger degree of disorder than the orthorhombic phases. With this in mind, we have chosen to explore the behaviour of three distinct types of model.

The first model consists of a regular array of infinite polymer chains, constructed through the use of periodic boundary conditions parallel to each of the cell axes. This is the most highly idealised model under consideration. The second model consists of finite, straight chains. The inclusion of chain ends increases the degree of realism. However, this model essentially is a representation of a short *n*-alkane system, and it is well known that segregation of the chain-ends in such systems can lead to chain tilting and the generation of alternative crystal phases that are not observed in polyethylene [31–34]. In order to prevent such effects, the starting configuration of the model has been disordered by sliding each chain by a random number of polyethylene *c*-cell repeats parallel to the chain axis, to eliminate any chain-end registration.

Both of these models were studied at elevated pressure (5 kbar) and a range of temperatures from 300 to 550 K, in which range the pseudo-hexagonal phase of polyethylene is known to form [1–6]. In each case, 48 chain stems were considered, arranged as shown in Fig. 1(a). For technical reasons (see below) it was necessary to restrict the models to a near cubic aspect ratio. Thus the infinite chain model effectively consisted of an array of $4\times6\times12$ unit cells of polyethylene, whereas the finite chain model consisted of a 4×6 array of unit cells, each containing two molecules of $C_{24}H_{50}$ in a herringbone arrangement. In each case the simulation box has approximate dimensions of $30\times30\times30$ Å.

The final model considered was introduced in a previous paper [23], and consists of a long chain which passes twice through the simulation box. This is made possible by the presence of a central jog, as shown in Fig. 2. It was indicated in our previous work that this model contains much of the disorder that might be expected in a real system and that, in particular, the jog mimics the effect of a chain-fold in a relatively small model. The jogged chain model is examined at ambient pressure only—the model forms a pseudo-hexagonal phase at 440 K prior to melting. The starting configuration is

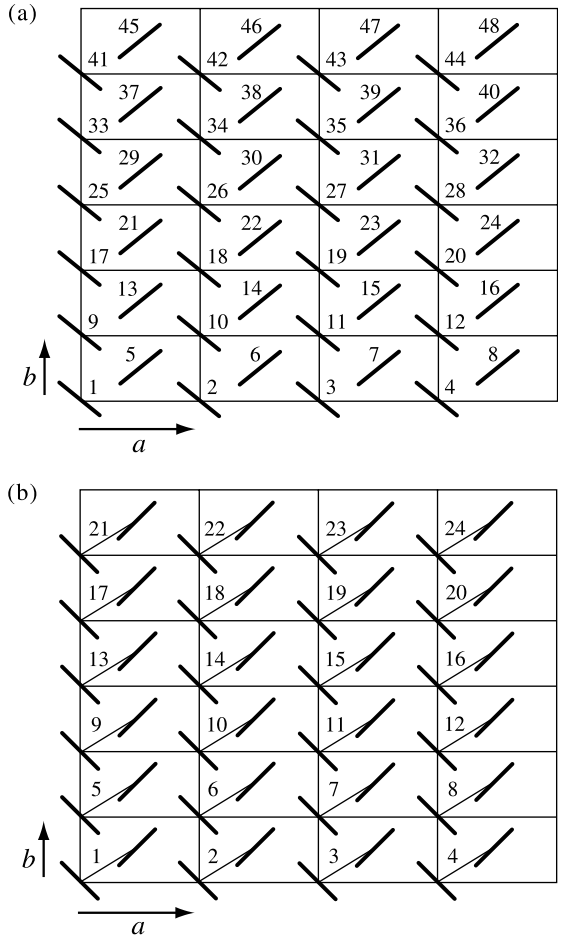

Fig. 1. (a) A schematic representation of the starting configuration for the $4\times6\times12$ infinite chain model, and the $4\times6\times C_{24}$ finite chain model, viewed looking down the *c* axis. (b) A similar view of the $4\times6\times C_{102}$ jogged chain model.

shown in Fig. 1(b) and has approximate dimensions of $30\times30\times60$ Å.

All models were constructed by replicating the published atomic coordinates (carbon atoms only) of Bunn [35] the appropriate number of times, and then editing where necessary to introduce chain ends and jogs. Hydrogen atoms were added in an ad hoc manner, and the energy of each structure was optimised, keeping the unit-cell parameters fixed, prior to the molecular dynamics simulations. The models and simulations performed are summarised in Table 1.

2.2. Molecular dynamics simulations

Molecular dynamics simulations were performed using the all-atom force field of Smith and Yoon [36] and the DL_POLY_2 program from the CCLRC [37]. All simulations were performed on a four processor Silicon Graphics Origin 200 computer. The choice of an all-atom method over united atoms has been discussed previously [23]: although unit-atom approaches have advantages of computational speed, they are unable to reproduce the orthorhombic phase of polyethylene adequately. The Smith and Yoon force field was chosen because of the strong emphasis the authors placed on determining the correct form of the backbone torsional potential—a key factor in the generation and propagation of *gauche* defects, which are expected to play a crucial role in the formation of pseudo-hexagonal phases.

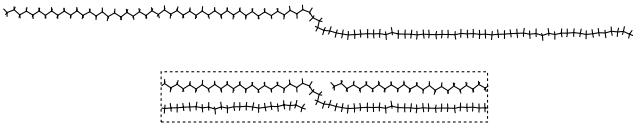

Fig. 2. A jogged chain of $C_{102}H_{206}$ shown in isolation (above) and confined to a periodic cell (below).

The Smith and Yoon force field has been used extensively in our previous simulations of linear and branched polyethylene crystals [23,38]. While it does not lead to a perfect agreement with experimentally determined lattice parameters, the discrepancies observed depend as much on the choice of model (i.e. infinite, finite or jogged chain) as on the choice of force field. By employing the same force field for the present study, we are able to examine the comparative behaviour of the different systems in both orthorhombic and pseudo-hexagonal phases.

Each simulation consisted of an equilibration period, and a production period. Equilibration was performed using the Berendsen isobaric-isothermal approach [39], and was continued until any systematic variations in the simulation cell dimensions appeared to have relaxed. The time needed for this to occur varied between the different models, with equilibration times up to 500 ps being required in some cases (Table 1). This is much longer than the time taken for thermodynamic variables such as energy and temper to equilibrate (typically $\lesssim$10 ps). Generally those simulations in which the final cell volume differed markedly from the initial volume (i.e. the high pressure simulations, and the simulation of the $4\times6\times C_{102}$ model at 440 K) required the longest equilibration time. The time constants for coupling the system to the temperature and pressure reservoirs, τ_T and τ_P were set to 0.4 and 8 ps, respectively. The reason for the large value of τ_P was to prevent rapid changes in cell dimensions that might cause the SHAKE algorithm to fail. The SHAKE algorithm was used to maintain constant bond lengths during the simulations [40,41]. Also for this reason, it was found necessary to restrict the anisotropy in the shape of the simulation box. For simulations at 5 kbar, it was necessary to employ a near-cubic box; at ambient pressure it was possible to use simulation boxes with an aspect ratio of 2:1, measured with respect to the chain-axis. A production time of 50 ps was used for all systems, with sampling in the microcanonical ensemble. The production period was long enough to give a consistent representation of the conformational behaviour of the chain stems, which was tested by repeating several of the simulations. However, a longer production time would enable the chain stem diffusion coefficients to be determined with greater accuracy. A 1 fs time step was used in all simulations.

Table 1
A summary of the models and simulations considered in the present study

Model	Chain type	Number of chains	Number of atoms	T (K)	Pressure (kbar)	Equilibration period (ps)	Production period (ps)
4×6×12 (infinite)	$-C_{24}H_{48}-$	48	3456	300	5	400	50
				350	5	300	50
				400	5	500	50
				450	5	300	50
				500	5	300	50
				550	5	300	50
4×6×C_{24} (finite)	$C_{24}H_{50}$	48	3552	300	5	400	50
				350	5	400	50
				400	5	400	50
				450	5	400	50
4×6×C_{102} (jogged)	$C_{102}H_{206}$	24	7392	300	0	100	50
				320	0	100	50
				340	0	100	50
				360	0	100	50
				380	0	100	50
				400	0	100	50
				420	0	100	50
				440	0	400	50

2.3. Analysis of torsions and setting angles

Conformational defects manifest themselves through changes in the torsions and setting angles present in the model. Frequency distributions are calculated both for the backbone torsions and for the setting angles. The setting angles are calculated for sub-units consisting of three consecutive methylene groups or carbon atoms. The setting angle of this three-methylene segment (3MS) is obtained by projecting the three backbone carbon atoms onto the basal plane of the unit cell (the x–y plane) and taking the angle between the bisector of the projected backbone bonds, and the x-axis, as illustrated in Fig. 3(a).

The evolution of individual torsional angles and defects may be followed by plotting all of the torsions and setting angles within a chain stem as a function of time, in a two dimensional map (adapting a method presented by Doherty and Hopfinger [42]). The value of each torsion or setting angle within a chain is plotted as a vertical line of colour pixels. A succession of such lines shows the evolution of the torsions or setting angles of the whole chain stem with time (Fig. 3(b) and (c)).

The colours have been chosen to give a clear colour difference between the different conformational states. For the torsional angles, the *trans* conformation is green, while the *gauche*$^+$ and *gauche*$^-$ conformations are blue and red, respectively. The transition from *trans* to *gauche*$^+$ is achieved via turquoise, while a similar transition to *gauche*$^-$ is via yellow. The colour table for the 3MS setting angles has six different colours, each indicating a

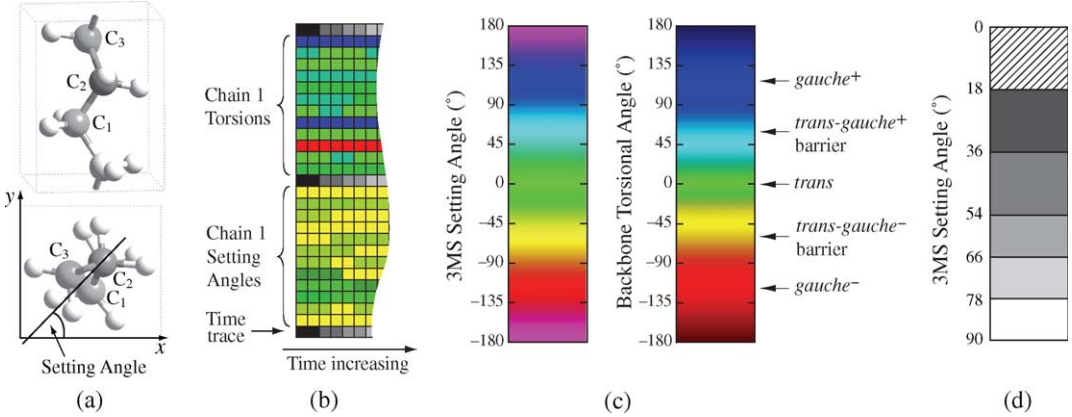

Fig. 3. (a) Definition of a 3MS setting angle. The co-ordinates of the carbon atoms are projected onto the x–y plane and the setting angle is defined as the angle between the bisector of the projected C_2–C_1 and C_2–C_3 bonds, and the x-axis. The angle is taken to be positive when increasing in the clockwise sense. (b) The colour maps used for displaying torsions and 3MS setting angles for a chain stem as a function of time. A vertical column represents the angles within a chain stem at a particular instant in time. The time evolution of a particular angle may be seen by following a horizontal line of colour. (c) The colour tables used in the colour maps. The setting angle colours are replaced by shades of grey when the 3MS is not aligned to the chain axis. (d) The grey scales used when the 3MS tilts away from the chain axis. Segments which are tilted by less than 18° are represented by the colour table shown in (c).

60-degree range. If a 3MS is tilted from the *c*-axis by more than 18° ($\cos^{-1}0.95$), the coloured pixels are replaced by a grey scale, used to indicate the degree of tilt of the 3MS from the chain axis (Fig. 3(d)).

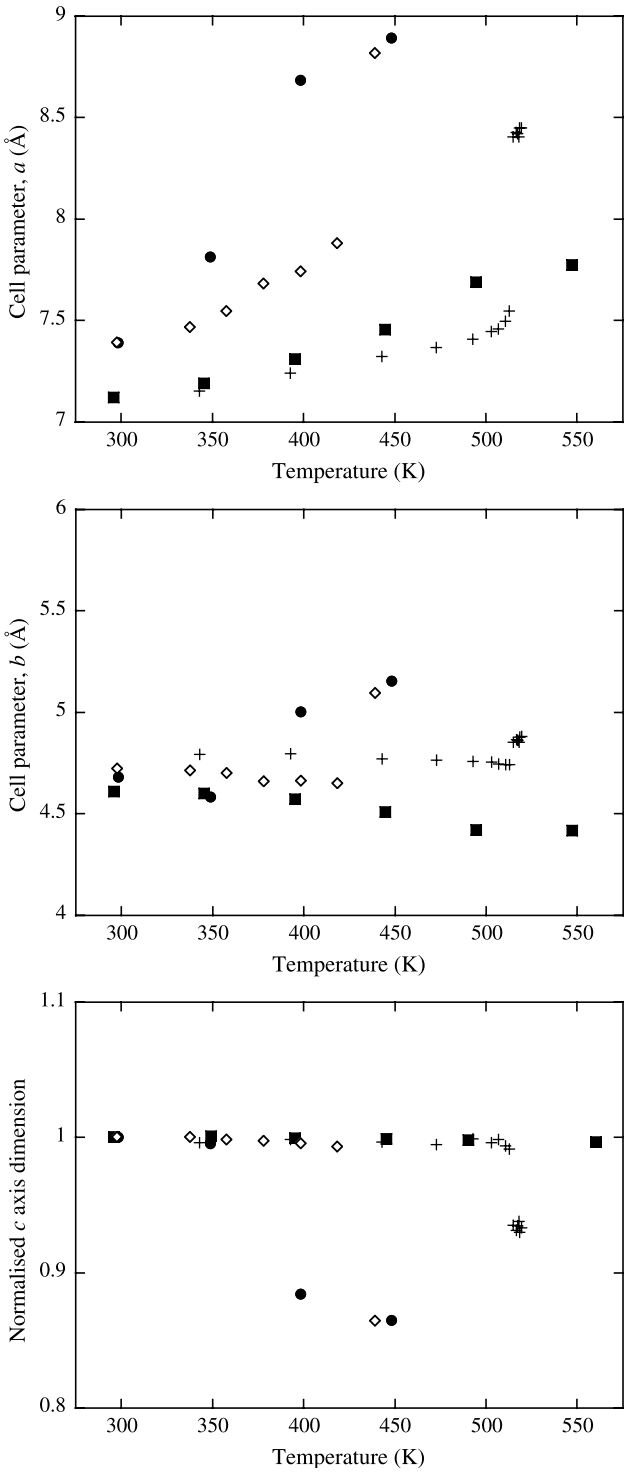

Fig. 4. The variation in the cell parameters *a* and *b*, and the normalised *c*-axis dimension, with temperature for the three models, compared with the experimental data from Yasuniwa et al. [4]. (■, infinite chain 4×6×12 model, 5 kbar; ●, finite chain 4×6×C_{24} model, 5 kbar; +, experimental data, 5 kbar; ◇, jogged chain 4×6×C_{102} model, ambient pressure).

3. Results

3.1. Lattice parameter variation

The variation in lattice parameters of the three models are shown in Fig. 4, compared with experimental data from Yasuniwa et al. [4] for a high density polyethylene sample with M_w=130,000 and a crystallinity of 94.2 wt%. As indicated above, the infinite chain (4×6×12) and finite chain (4×6×C_{24}) models were simulated at 5 kbar, while the jogged chain (4×6×C_{102}) model was simulated at ambient pressure. The experimental data were also obtained at a nominal pressure of 5 kbar. Absolute values of the *c* parameter are not shown. Instead, the simulation box dimension parallel to the chain axis was recorded, and normalised to the value at 300 K. The reason for this approach is that the crystallographic *c* repeat is not well defined when the system enters a mobile phase, and is difficult to measure unambiguously from a simulation. The ratio of cell parameters *a*/*b* is plotted in Fig. 5.

All three models exhibit the expected trend in which the *a* parameter increases rapidly relative to *b*, as the temperature is increased. However, the manner in which the change occurs is different in each case. It is helpful first of all to consider the experimental data; this provides a standard against which the models may be compared.

The experimental *a* parameter increases gradually up to about 520 K, where-upon it jumps from about 7.6 to 8.4 Å. The sudden increase in *a* is accompanied by a more modest jump in *b*, and a 7% decrease in the *c* parameter. The ratio of *a*/*b* jumps to 1.73, i.e. the value expected for a pseudo-hexagonal phase.

The increase in both *a* and *b* implies an increase in the basal area of the unit cell, and the simultaneous decrease in *c* is interpreted as meaning that the polymer backbones contain a large number of conformational defects and possesses a larger cross-sectional area [4,5]. In this respect, polyethylene differs from the behaviour of the shorter *n*-alkanes, which form rigid

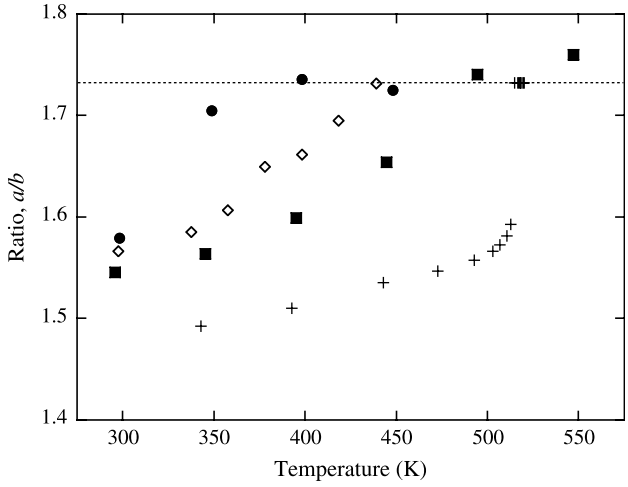

Fig. 5. The variation in cell parameter ratio *a*/*b* with temperature for the three models compared with the experimental data from Yasuniwa et al. [4]. (■, infinite chain 4×6×12 model, 5 kbar; ●, finite chain 4×6×C_{24} model, 5 kbar; +, experimental data, 5 kbar; ◇, jogged chain 4×6×C_{102} model, ambient pressure). The dotted line corresponds to a ratio of $\sqrt{3}$.

rotator phases consisting mainly of all-*trans* sequences [31,33,43–46]. The pseudo-hexagonal phase in polyethylene is stable over a relatively narrow temperature range, after which melting occurs.

For the infinite model the changes in the cell parameters follow similar trends to those seen in real systems at lower temperatures. However, as the temperature increases the ratio of the cell parameters (*a*/*b*, see Fig. 5) moves smoothly towards the hexagonal case ($\sqrt{3}$), without a sudden jump. It is also apparent that there is no sudden increase in the *a* parameter, and no drop off in the value of the *c* parameter. It has been commented previously [23] that infinite chain models are unrealistic because the periodic boundary conditions prohibit individual chains from contracting relative to their neighbours, with the consequence that conformational defects, i.e. *gauche* conformations, are rare. It would appear likely that the same effect is occurring here; the chains are unable to contract in the *c* direction, and instead, behave as rigid rotors. This hypothesis will be examined further below.

The behaviour of the finite chain model is quite different from the infinite case. The *a* parameter is larger than the experimental value at 300 K, and increases rapidly, so that at 400 K it already exceeds the value for the experimental pseudo-hexagonal phase. The *b* parameter also shows large changes, and the ratio *a*/*b* reaches 1.71 at 350 K, rising further to 1.73 at 400 K and above. Curiously, the *c* parameter shows little decrease at 350 K, but drops by 12% at 400 K, raising the possibility that this system may exhibit two different pseudo-hexagonal phases: an extended chain or rigid rotor phase at 350 K, and a contracted chain phase at 400 K and above.

In some ways the behaviour of the jogged chain model is closest to the experimental behaviour, albeit that the simulation is performed at ambient pressure rather than 5 kbar. The *a* parameter rises steadily over a wide temperature range, and then jumps up in value as a pseudo-hexagonal phase is formed at 440 K. It should be expected that an increase in pressure would decrease the *a* parameter, and increase the transition temperature to bring the simulation in line with experiment. The jogged chain simulation also shows a sharp rise in *b* parameter, and a sharp decrease in *c*, on entering the pseudo-hexagonal phase, consistent with the formation of the contracted chain phase described above. Another similarity with the experimental work, not obvious from the graphs, is that the pseudo-hexagonal phase has a narrow range of stability: the structure is lost on increasing the temperature to 460 K.

Although the description of the pseudo-hexagonal phases formed by the different models has been made purely on the basis of changes in the unit cell parameters, evidence will be presented below, based on an examination of the torsions and setting angles within each structure, to confirm the designation of each phase as either a rigid rotator or a contracted-chain phase.

3.2. Torsions and setting angle distributions

The torsion and setting angle distributions for the three models are shown in Figs. 6 and 7, respectively. The torsional distributions are consistent with the observations made in the previous section. In the case of the infinite chain (4×6×12) model, the distribution consists entirely of *trans* conformations at all temperatures. The only variation seen is that the distribution gradually broadens as the temperature increases. On the other hand, the finite chain (4×6×C_{24}) model has an all-*trans* distribution at 300 and 350 K, but at 400 K and above

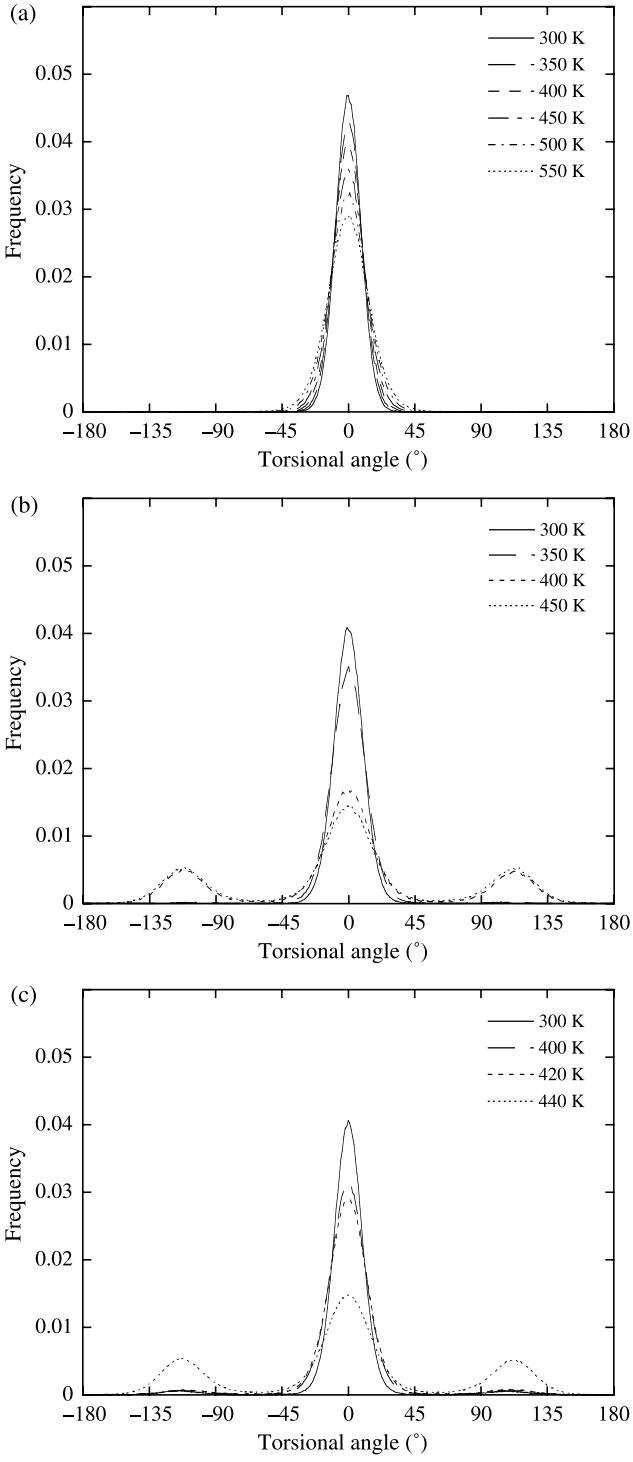

Fig. 6. The distribution of torsional angles with temperature for (a) the infinite chain (4×6×12) model at 5 kbar, (b) the finite chain (4×6×C_{24}) model at 5 kbar and (c) the jogged chain (4×6×C_{102}) model at ambient pressure.

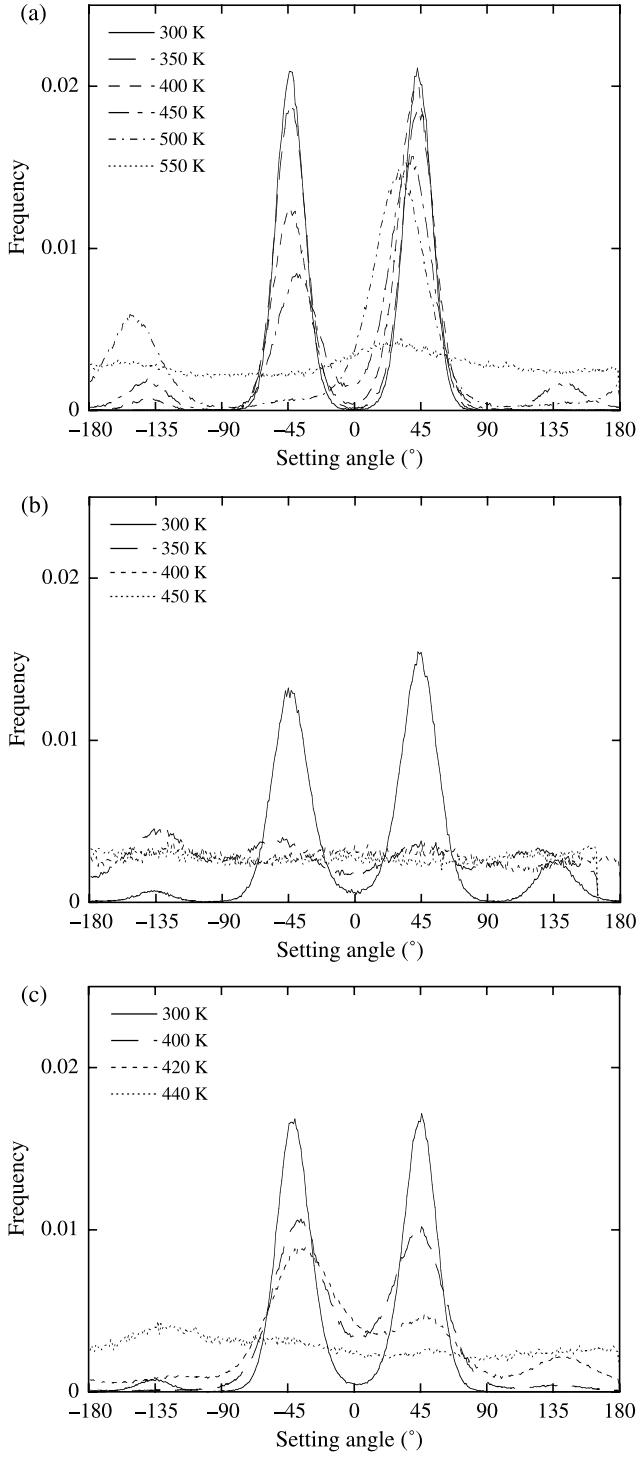

Fig. 7. The distribution of 3MS setting angles with temperature for (a) the infinite chain (4×6×12) model at 5 kbar, (b) the finite chain ($4\times6\times C_{24}$) model at 5 kbar and (c) the jogged chain ($4\times6\times C_{102}$) model at ambient pressure.

the distribution contains a significant proportion of *gauche*$^+$ and *gauche*$^-$ conformers, consistent with the formation of the contracted chain pseudo-hexagonal phase. Similar behaviour is observed in the jogged chain ($4\times6\times C_{102}$) model: although small proportions of *gauche* conformations are seen at 400 K, the most significant change occurs at 440 K when the distribution takes on an appearance very similar to that of the finite chain model at 450 K.

The setting angle distributions also support the pseudo-hexagonal phase designations made previously. The infinite chain setting angles are shown in Fig. 7(a). Although the chains remain close to the all-*trans* planar zigzag, there are significant changes in the chain packing. At 300 and 350 K the chains remain in the herringbone packing of the starting structure, as indicated by two strong peaks centred around $\pm45°$. By 400 K occasional chain rotations are beginning to occur, and by 450 K there are clearly four preferred setting angles, characteristic of herringbone packing with some of the chains rotated by π radians about their long axes. The structure is dominated by herringbone packing until 500 K, when a transition to a monoclinic type of packing occurs. The monoclinic packing is characterised by all of the chain setting angles being parallel, which appears in the distribution as two peaks separated by 180°. However, this order breaks down to a near-uniform distribution of 3MS setting angles at 550 K, corresponding to the onset of the pseudo-hexagonal phase.

The behaviour of the finite chains model is somewhat simpler. As before, there is clear evidence for herringbone packing at the lowest temperature. However, at 350 K, the temperature of the rigid rotator phase, the setting angle distribution becomes almost uniform, albeit with four small peaks corresponding to the four orientations possible in herringbone packing. It should be remembered that the unit cell was not quite hexagonal at this temperature ($a/b=1.71$ rather than 1.73), and so it appears that the rotations are not completely free at this temperature. At 400 K and above, the distribution is uniform, and the system has transformed to a freely-rotating contracted-chain pseudo-hexagonal phase.

The jogged chain model behaves similarly to the finite chain model, with two important distinctions. First, there is no extended chain (rigid rotor) phase, and second, although the setting angle distribution at 440 K is uniform, it should not be inferred that rotation of the chain stems is completely free. The chain stems in the jogged chain model are constrained by the presence of the jog, just as they are in real crystals by the presence of chain folds. So, although there is undoubtedly dynamic rotational disorder, for which further evidence will be presented shortly, it is not possible for an entire chain stem to rotate unhindered through 360°.

3.3. Setting angle correlation functions

The setting angle correlation functions indicate the extent to which the individual 3MS units along a particular chain stem are correlated. A high value for this function, extending a significant distance along the chain stem, is an indication that the stem is behaving as a rigid unit when it rotates. The correlation functions for the three models are shown in Fig. 8. At 300 K, the infinite chain (4×6×12) model shows a rapid drop in correlation between the 3MS units with distance along the chain, so that 3MS units which are six or more units apart are essentially uncorrelated (Fig. 8(a)). It should be borne in mind that, at this temperature, the amplitude of motion will be

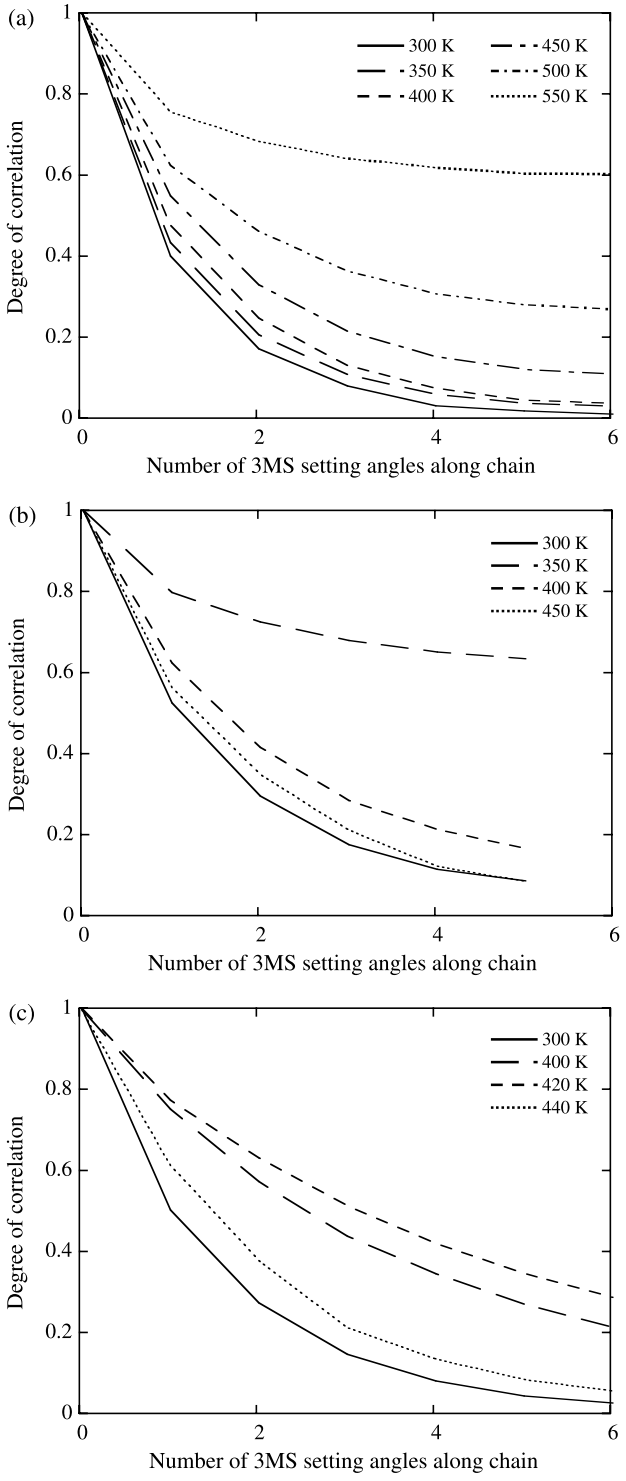

Fig. 8. The linear intra-chain angular correlation function between 3MS setting angles, for various temperatures, for (a) the infinite chain (4×6×12) model at 5 kbar, (b) the finite chain ($4\times6\times C_{24}$) model at 5 kbar and (c) the jogged chain ($4\times6\times C_{102}$) model at ambient pressure.

very small, and the behaviour seen is due to random, thermal vibrations. However, as the temperature is increased, the extent of correlation increases, reaching a value of 0.6 (for a separation of 6×3MS units) when the system enters the pseudo-hexagonal phase at 550 K. This is clear evidence, therefore, that the motions of the 3MS units in each chain stem are correlated, and, although the correlation is not perfect, we may suggest that the chains are behaving at least as semi-rigid rotors when in the pseudo-hexagonal phase of the system.

The finite chain ($4\times6\times C_{24}$) systems show a markedly different behaviour from the infinite ones (Fig. 8(b)). At 300 K the degree of correlation is low, but greater than that of the equivalent infinite system. It would appear that the introduction of chain ends increases the freedom of the chain to rotate in a concerted fashion. However, on increasing the temperature to 350 K, we observe a marked increase in the correlation function, to a value which is higher than for any other system simulated. Again, this provides evidence that the system is behaving as a set of semi-rigid rotors. At 400 K and above, the correlations die away again, which is consistent with the formation of the conformationally disordered contracted-chain pseudo-hexagonal phase.

The behaviour of the jogged chain ($4\times6\times C_{102}$) model (Fig. 8(c)) is quite similar to that of the finite chain system, though less extreme. The correlations show an increase at 400 and 420 K, indicating a level of concerted libration of the 3MS units. Once again, however, on entering the conformationally disordered pseudo-hexagonal phase, the correlations are lost.

Thus, the correlation functions shown in Fig. 8 clearly emphasize the distinction between the two types of pseudo-hexagonal phase. In the extended-chain phases, as observed in the infinite chain system at 550 K and in the finite chain system at 350 K, the chain stems behave as semi-rigid rotors. On the other hand, in the contracted-chain systems, (e.g. the finite chain system at 400 K and above, and the jogged chain system at 440 K) the chains are conformationally disordered: there is no evidence for strong correlations between the 3MS setting angles, and any motions of the 3MS units take place in an unconcerted manner. Although the symmetry of the phase implies rotational disorder, there is no indication from these results that it is dynamic.

3.4. Dynamics of individual torsions and setting angles

An examination of the colour maps, described in the methods section, gives the opportunity to examine the behaviour of individual torsions and setting angles within each model, and in particular to observe the dynamics of each system. Colour maps were produced for each of the chains in each model, under each condition of temperature and pressure. They will be discussed here in turn; only a few representative maps will be shown, in order to illustrate particular types of behaviour.

3.4.1. Infinite chain model

Colour maps for a typical chain taken from the infinite chain (4×6×12) model are shown in Fig. 9. At 5 kbar and 300 K, there is little activity in the infinite chain model; the chains are all-*trans* and the stems remain in the herringbone packing of the starting structure. Fig. 9(a) shows the colour maps for chain 2 from this simulation. The green of the torsional map is indicative of *trans* conformations, while the cyan colour of

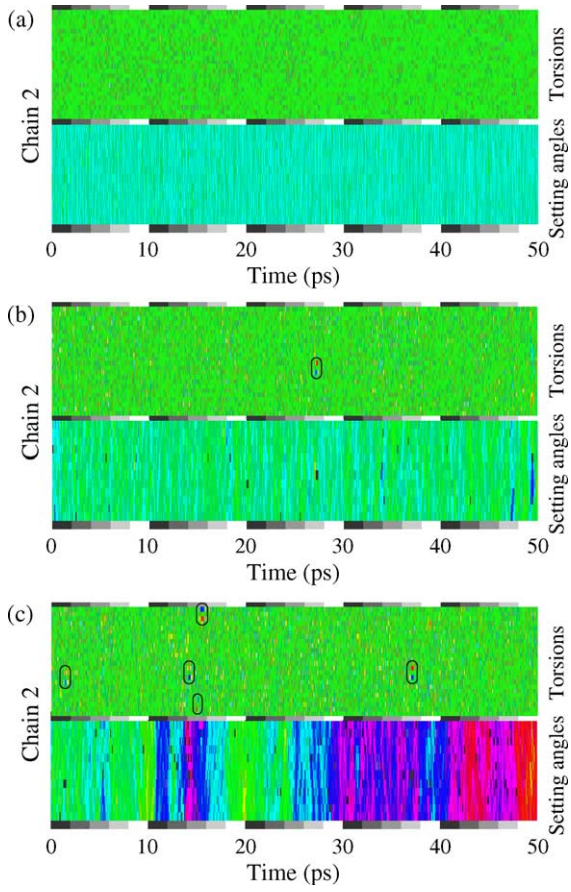

Fig. 9. The colour maps representing the torsional and 3MS setting angles for a typical chain from the infinite chain (4×6×12) model during the 50 ps production runs at 5 kbar: (a) 300 K, (b) 500 K and (c) 550 K. The colour tables used are given in Fig. 3 and the chain numbering is given in Fig. 1(a). A number of $g^{-}tg^{+}(2gl)$ defects are highlighted.

the setting angle map indicates that all of the 3MS units are oriented at a setting angle of +45°. Slight fluctuations in colour are indicative of low amplitude librations.

On increasing the temperature, little change is observed, apart from a gradual increase in the amplitude of the rotational librations. At 400 K and above (not shown), occasional chain-flips are observed, in which a small group of chains, typically up to six at a time, simultaneously change setting angle from +45 to −45°, or vice versa. Such flips are relatively infrequent, occurring perhaps once or twice in each 50 ps simulation, but highlight the need for co-operativity in rotational changes at low temperatures.

It was pointed out when examining the setting angle distributions (Fig. 7) that the 500 K simulation adopts a monoclinic type of packing arrangement, in which all setting angles are equal, or related by a π rotation about the chain axis. This transition occurs during the equilibration period and is not an indication of any great change of mobility in the system. In fact, as can be seen in Fig. 9(b), the behaviour of the chains has changed little from that at 300 K. All that may be observed is that there is a modest increase in the amplitude of librations, accompanied by a slight increase in the level of disorder. This is manifested in the figure by a very rare *gauche*$^{-}$–*trans*–*gauche*$^{+}$ ($g^{-}tg^{+}$ or $2gl$) defect, and the fact than a small proportion of 3MS units are tilted away from the chain axis (indicated by grey spots). There is a further indication of co-operative rotation (not shown), in which a group of six chains, starting with chain 5, and working up and down a column in sequence with chains 13, 45, 21, 29 and 37 (Fig. 1(a)), flips into a herringbone packing arrangement.

At 550 K, the rotational behaviour of the chain stems in the infinite model changes dramatically, as can be seen very clearly in Fig. 9(c). The setting angle map shows bands of colour sweeping up and down the chain as it rotates through a full 360° during the period of the simulation. Despite the enhanced mobility, the chains are still substantially within the all-*trans* conformation and only brief conformational defects (circled) are in evidence. The colour map thus provides clear evidence for the formation of an extended-chain rotator phase, in which the polymer chains rotate as nearly rigid units, while maintaining an all-*trans* conformation.

3.4.2. Finite chain model

As has already been noted from the angular distributions (Figs. 6 and 7), the finite chain (4×6×C_{24}) model contains considerably more conformational activity at 300 K and 5 kbar than the infinite chain model. This is highlighted by an examination of the angular colour maps (Fig. 10). Chain 6 is

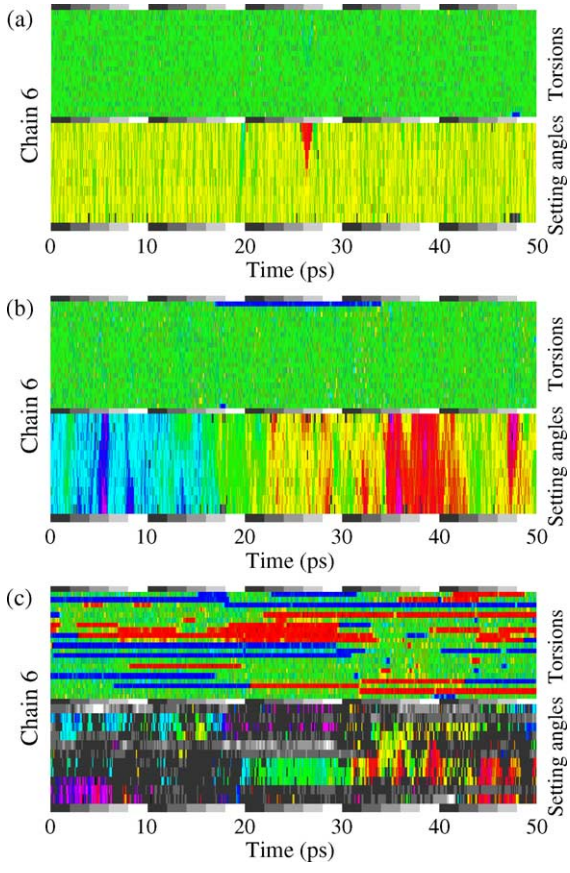

Fig. 10. The colour maps representing the torsional and 3MS setting angles for a typical chain from the finite chain (4×6×C_{24}) model during the 50 ps production runs at 5 kbar: (a) 300 K, (b) 350 K and (c) 400 K. The colour tables used are given in Fig. 3 and the chain numbering is given in Fig. 1(a).

shown at three different temperatures. At 300 K, setting angle fluctuations are observed, the colour range from yellow to green representing setting angles between −70 and 0°. The influence of the chain ends is also apparent, with a partial chain rotation propagating from the top end of the chain at about 26 ps into the simulation. Chain end defects are also seen: in chain 6, there is a single *gauche*$^+$ state at 38 ps, with a corresponding tilt of the chain-end 3MS away from the chain axis (indicated by grey pixels).

At 350 K (Fig. 10(b)) the colour maps are very similar to those of the infinite chain model at 550 K (Fig. 9(c)). The evidence for the extended-chain rotator phase is again clear. The main difference between the two systems is the possibility of chain-end defects in the finite chain case, which often induce the start of a twist motion, which then propagates along the chain. In the infinite case, this does not occur. Chain rotations, whether successful or abortive, can begin at any point along the chains, but are limited in amplitude by the connectivity of the chain and the periodic boundary conditions. In the finite case, if a chain rotation begins at one end of the chain, it is possible to build up a very large degree of twist along the chain. For example, Fig. 11 shows a detailed view of chain 7, taken from the finite chain simulation at 350 K, which contains a twist of 120° extending along most of the chain stem. This is the largest degree of twisting seen in the extended-chain phases and can be contrasted with the 'UTAH twist' [47–49], a smooth 180° twist extending over 12 carbon atoms, which was proposed to explain dielectric measurements.

At 400 K, the colour maps change dramatically (Fig. 10(c)). The previously green all-*trans* torsional angle colour maps are now characterised by significant proportions of *gauche*$^+$ (blue) and *gauche*$^-$ (red) conformational defects, whereas the 3MS setting-angle colour maps are dominated by the greys that indicate the degree to which chain segments are tilted away from the average-chain axis. This is the contracted-chain pseudo-hexagonal phase. Where aligned 3MS units occur, their colours change frequently throughout the simulation, indicating that the structure formed is not static, but constantly changing. It is reasonable, therefore, to describe this phase also as a 'rotator' phase. No further changes are observed in the colour maps on heating to 450 K.

3.4.3. Jogged chain model

The colour maps for the jogged chain ($4\times6\times C_{102}$) model, up to 400 K, were examined in some detail in a previous publication [23]. We will restrict our comments to the highest temperatures simulated (Fig. 12). At 420 K, and ambient pressure, the torsional distribution is predominantly green, indicating *trans* conformations. The band of torsional defects (red and blue) across the centre of the plot correspond to the position of the jog; other g^-tg^+ and chain-end defects are also evident. In fact, the uniformity of the torsional plot belies the complexity of the setting angle map, which shows frequent twist defects propagating both from the chain ends and from the central jog. Despite this level of activity, the two halves of the chain-stem end the simulation with the same setting angles as they begin it. This is not the case generally, however, and rotational flips are regularly observed between the four angles consistent with herringbone packing.

At 440 K, the system enters the contracted-chain pseudo-hexagonal phase. The colour maps (Fig. 12) appear very similar to those of the finite chain model at 400 K and 5 kbar

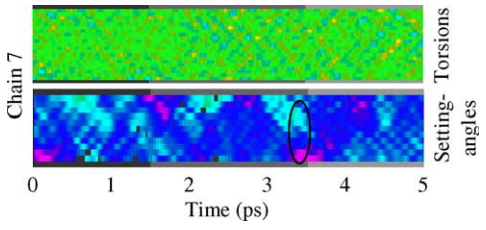

Fig. 11. A detailed section of the colour maps for the torsional and 3MS setting angles of chain 7 from the 350 K 5 kbar production run of the $4\times6\times C_{24}$ finite chain model. The colour tables used are given in Fig. 3 and the chain numbering is given in Fig. 1. A 120° twist is highlighted.

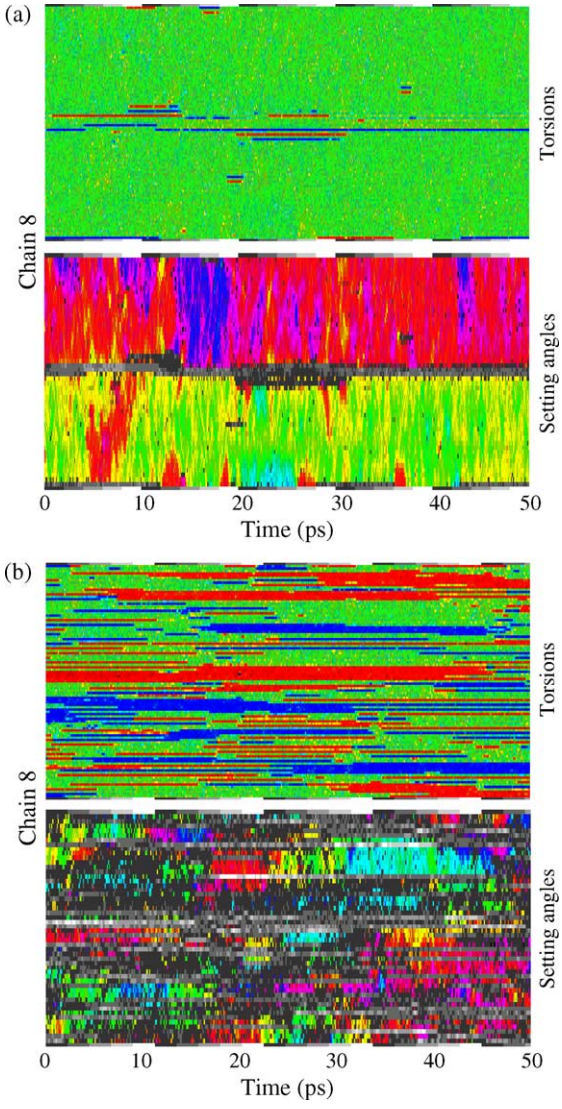

Fig. 12. The colour maps representing the torsional and 3MS setting angles for a typical chain from the jogged chain ($4\times6\times C_{102}$) model during the 50 ps production runs at ambient pressure: (a) 420 K and (b) 440 K. The colour tables used are given in Fig. 3 and the chain numbering is given in Fig. 1(b).

pressure (Fig. 10(c)). As before, the torsional map is dominated by *gauche*$^+$ and *gauche*$^-$ defects (blue and red pixels), and the setting angle map shows that a significant fraction of each chain is tilted away from the average *c*-axis of the system (grey pixels). As with the finite chain system, the variation in colour of the setting angle map indicates that the disorder is of a dynamic nature. It is clear, however, that the phase cannot be thought of as freely rotating, because each chain-stem is still constrained by the presence of the jog.

3.5. Spatial distribution of the 3MS units

Much has been learnt about the conformational and rotational order by studying distribution functions and colour maps. However, one important aspect of the pseudo-hexagonal phases is that they are thought to confer mobility on the polymer chains, and this feature of our models still remains to be examined. In this section, we will consider spatial distribution functions for the 3MS units, in order to gauge the extent to which they deviate from their lattice sites during each simulation. This will be supplemented in the next section by direct calculations of transport coefficients parallel to the chain axes.

The distribution functions shown below are two dimensional sections through a three-dimensional histogram of neighbour distances for each 3MS unit. The plane of the section is chosen to include the [110] and [001] lattice vectors. The functions effectively demonstrate the level of positional disorder present both parallel and perpendicular to the chain axes. Each distribution function is averaged over the whole of each 50 ps production run.

3.5.1. Infinite chain model

Fig. 13 shows the 3MS spatial distribution functions at 5 kbar for the infinite chain (4×6×12) models. It can be seen that the 3MS are constrained to their lattice sites for the temperature range 300–400 K. From 450 to 550 K the distribution broadens in the chain axis direction. As the model contains very few *gauche* defects, this cannot be due to kinking of the chains. Instead the spread of the distributions implies that the chains are oscillating up and down in the chain axis direction. In the case of the 550 K production run, the spread is so great that adjacent locations along the chains coallesce and chain sliding is implied.

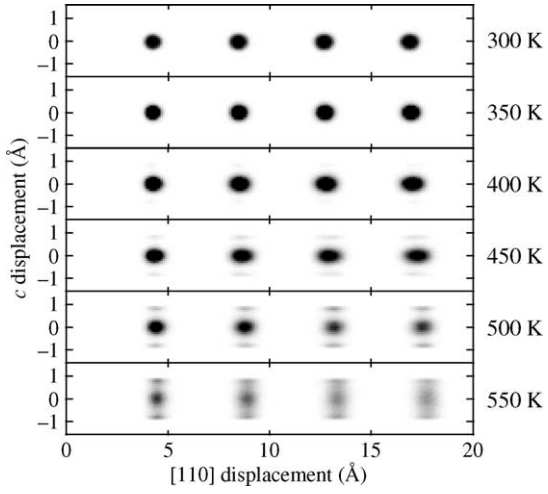

Fig. 13. Plots of the 3MS spatial distribution functions for the infinite chain (4×6×12) model, as a function of temperature, at a pressure of 5 kbar.

The plot of the spatial distribution function at 450 K also indicates a broadening of the distribution in the [110] direction (Fig. 13). By referring to other sections through the spatial distribution function, we have determined that the spread is actually parallel to the *y*-axis. This could be related to a type of disorder found in polyethylene crystals and commented on, separately, by Dorset [50] and Busing [51].

Dorset noted longitudinal chain static displacements of up to 0.25 Å in the *b* direction, 'frozen in' at low temperatures, for polyethylene and *n*-paraffins. This conclusion was drawn from a consideration of the diffuse scattering noted along the *a*-axis in electron diffraction patterns.

On the other hand, Busing found elongation of the atomic thermal ellipsoids after full pattern refinement of X-ray diffraction data taken from highly drawn fibres of ultra-high molecular weight (4×10^6) polyethylene. It was concluded that the thermal displacements were the same in the *a* and *b*-axes, but that there appeared to be additional chains between the chain sites along the *b*-axis direction. The fractional occupancy of these interstitial positions was calculated to be less than 0.1.

In the present case, Busing's model cannot apply because the lateral positions of the chains are not observed to change; the behaviour appears consistent with that suggested by Dorset. The precise cause may be the presence of a small proportion of chains in the simulation that have flipped out of the normal herringbone packing. The distortion reaches a maximum during the 450 K simulation and then decreases as the pseudo-hexagonal phase is approached.

3.5.2. Finite chain model

The spatial distribution function provides further evidence for the increased activity of the finite chain (4×6×C_{24}) model compared with the infinite chain model. In the extended-chain pseudo-hexagonal phase (350 K and 5 kbar, see Fig. 14),

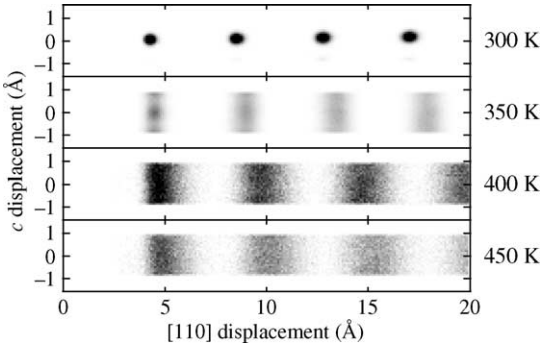

Fig. 14. Plots of the 3MS spatial distribution functions for the finite chain (4×6×C_{24}), model, as a function of temperature, at a pressure of 5 kbar. The distribution functions have been calculated using the same greyscales as for the infinite chain model (Fig. 13), except for the 400 and 450 K plots, in which the range is 40 times smaller.

the first nearest neighbour distribution shows a faint spot on a diffuse background, indicating that there is only partial registration between the 3MS units. However, the second and more distant neighbour distributions show no indication of any registration at all. As with the infinite chain model at 550 K, we may infer that chain sliding is occurring. The lateral shapes of the distribution peaks show only modest broadening, suggesting that the chains remain close to their lattice sites in the extended-chain rotator phase.

At 400 K the order within the system is markedly reduced: the breadth of the distributions in the [110] direction has increased compared to the distribution at 350 K and the distributions appear uniform in the chain axis direction. This provides clear evidence for the complete loss of chain registration in the chain axis direction, a feature that is characteristic of the high-pressure mobile phases of polyethylene. The trend continues at 450 K, with an increased spacing and diffuseness of the distributions.

3.5.3. Jogged chain model

The distribution functions for the jogged chain ($4\times6\times C_{102}$) models at ambient pressure are shown in Fig. 15. The curious doubling of the first and third neighbour distributions at 300 K is due to the fact that the different parts of the chain-stem on either side of the jog are not exactly superimposed on their lattice sites. The effect was noted previously [23], and disappears on heating. At 420 K the model still appears to be well ordered, with clear peaks in the distribution out to the fourth nearest neighbour. The transition to the contracted-chain rotator phase corresponds to a marked change in the distribution; the appearance is very similar to that occurring in the finite chain system at 400 K and above, and the same conclusions may be drawn concerning chain mobility.

The distribution functions for the four rotator phases simulated are summarised in Fig. 16, together with a similar plot taken from a branched-chain system described in Ref. [38] (see below). The most obvious similarity is that all of the rotator phases feature a degree of chain mobility parallel to the chain axis, characterised by a blurring of the function in the *z*-direction.

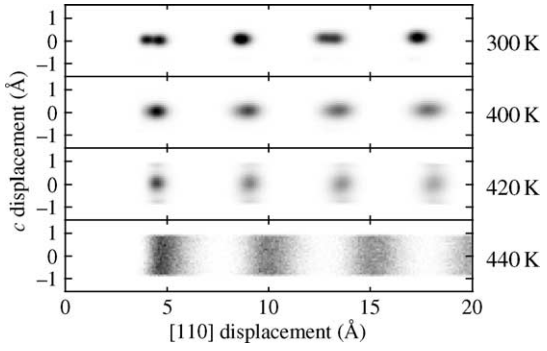

Fig. 15. Plots of the 3MS spatial distribution functions for the jogged chain ($4\times6\times C_{102}$) model, as a function of temperature, at ambient pressure. The distribution functions have been calculated using the same greyscales as for the infinite chain model (Fig. 13), except for the 440 K plot, in which the range is 40 times smaller.

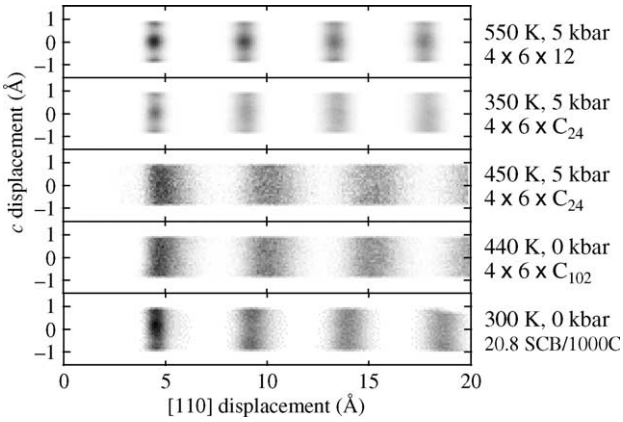

Fig. 16. A summary of the 3MS spatial distribution functions for the four pseudo-hexagonal phases observed during the present simulations, together with a similar plot for the branched-chain system described in Ref. [38] (see text).

However, the distributions also show a clear difference between the behaviours of the two types of rotator phase. In the extended-chain, rotator phases (infinite chain model at 550 K and finite chain model at 350 K), there remains a partial registration between the monomer units on adjacent chains, and the chains continue to pack quite regularly. However, in the contracted-chain rotator phases (finite chain model at 450 K and jogged chain model at 440 K), the conformational disorder of each chain causes it to have an irregular shape. This leads to both a decrease in packing order, and a loss of registration between chains. We might expect, therefore, that the chain mobility within the contracted-chain phases will exceed that in the extended-chain phases: this point will be addressed in the next section.

The distribution functions also reveal that there is a stronger degree of order in the chain axis direction in the infinite chain model at 550 K, than in the finite chain model at 350 K. This is entirely consistent with our observations on the angular distributions and colour maps of these phases which emphasise the degree to which the infinite chain model is constrained by the periodic boundary conditions.

The results from the branched chain model [38] are included for completeness. The simulation consisted of a finite chain ($4\times6\times C_{24}$) model with 20.8 ethyl side-chain branches added per 1000 backbone carbon atoms. This amounted to one side branch per chain stem, which had the effect of artificially lowering the density of the system. The simulation was performed at 300 K and ambient pressure. The appearance of the 3MS distribution function bears some resemblance to both the extended-chain and the contracted-chain phases: the first nearest neighbour has a peak superimposed on a diffuse background, indicating local chain registration, while the higher order peaks are laterally broader than those of the extended-chain model. Also, the positions of the higher order peaks are intermediate between those of the two models. This type of behaviour is perhaps not surprising, given that the system was found to include both fully extended, all-*trans*, chains and chains which were dominated by *gauche* defects.

3.6. Transport coefficients

Although chain sliding is indicated by the spatial distribution functions (Fig. 16), this has not yet been quantified. By calculating a transport coefficient from the z co-ordinates of the 3MS units, a measure of the rate of chain sliding (parallel to the chain axis) can be obtained. The transport coefficients are calculated from half the gradient of $\langle (z(0)-z(t))^2 \rangle$ plotted against time, where $\langle (z(0)-z(t))^2 \rangle$ is averaged over all possible starting points on each chain within the model, $z(0)$, and over all possible starting times [41].

Table 2 contains the transport coefficients calculated for the three models at different temperatures. Chain sliding is only observed when the system is in a pseudo-hexagonal phase. The general observation is that the transport coefficient is greater in the contracted-chain phases than in the extended-chain ones, which is consistent with the observation that the extended-chain phases possess a greater degree of registration between monomer units on adjacent chains. As a particular example, the contracted-chain phase of the finite model has a transport coefficient between 5 and 8 times greater than the extended-chain mobile phase of the same system.

The diffusion coefficients quoted in Table 2 are quite large compared with experimental values. For example, de Langen and Prins quote a value around 2×10^{-5} Å^2/ps for polyethylene in the pseudo-hexagonal phase [10]. The difference may be attributed to the fact that we are considering the diffusion of low molar mass constituents, rather than long polymer chains in a chain-folded lamella. Nevertheless, the values in the table provide a useful guide to the relative chain mobilities in the different phases.

The transport coefficients for the jogged chain model show that although chain sliding begins on entry to the contracted-chain phase it occurs to a lesser degree than in the finite chain case. This is probably because motion of the jogged chain motif used to construct the model requires the simultaneous movement of both halves of the chain in the same direction.

Table 2
Table of transport coefficients for chain sliding parallel to the chain axis direction

Model	T (K)	Pressure (kbar)	Transport coefficient (Å^2/ps)
4×6×12 (infinite chain)	450	5	0.00
	500	5	0.00
	550	5	0.08
4×6×C24 (finite chain)	300	5	0.00
	350	5	0.08
	400	5	0.43
	450	5	0.67
4×6×C_{102} (jogged chain)	420	0	0.00
	440	0	0.11
Branched model (20.8 SCB/1000C)	300	0	0.05

The data for the branched model has been taken from Ref. [38] (see text).

The transport coefficient for the branched model, introduced in the previous section, is the lowest of all of the rotator phases, at 0.05 Å^2/ps. This may be a consequence of the low temperature (300 K) at which the phase occurs, since it is clear from Fig. 16 that the density of the branched phase is lower than the extended-chain rotator phases, which would otherwise be expected to promote chain sliding.

The differences in character of the chain sliding motions, in the extended-chain and contracted-chain phases, can be seen in Fig. 17. In this figure the centres of mass of two arbitrary 3MS units are plotted as a function of time. The graph gives an impression of the more continuous motion of the contracted-chain phase (dotted lines), compared with the steps and plateaux of the extended chain phase (solid lines), and also indicates the different amplitudes of motion in each case.

4. Discussion

In this paper, we have attempted to simulate the mobile phase of polyethylene. To achieve this, we have made use of computer models, which were, of necessity idealised in various ways, in order to reproduce complex behaviour using a relatively small model. In fact, all of the models employed chain-stems, which were short compared to the lengths found in typical chain-folded lamellae. However, despite the apparent deficiencies of the models, it has proved possible to capture the essence of the mobile phase, both structurally and dynamically, and in so doing, we have been able to obtain insights into the conformations and motions of the molecules within the crystalline and mobile phases of these systems.

The modelling presented has identified two distinct types of mobile phase that occur under differing conditions. The extended-chain pseudo-hexagonal phase occurs in both the infinite (4×6×12) and finite chain (4×6×C_{24}) models under high pressure and elevated temperatures. The contracted-chain phase also occurs in the finite chain model at high pressure and in the super-heated jogged-chain (4×6×C_{102}) model at ambient pressure. A third phase, of intermediate character,

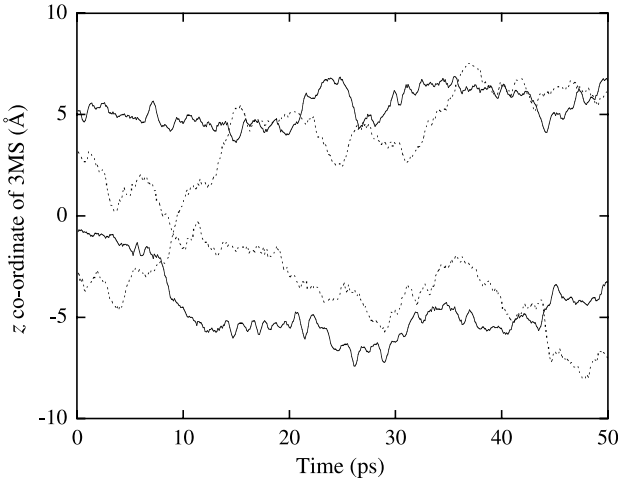

Fig. 17. The z positions of the centres of mass of two 3MS units, taken from the 4×6×C_{24} model, plotted versus time during a 50 ps production run, at 350 K (solid lines) and 450 K (dotted lines), and 5 kbar pressure.

was also found in a somewhat artificial, highly branched system. Table 3 includes a list of all of the mobile phases found, and the conditions under which they occur.

The contracted-chain mobile phase shows the features characteristic of the high-pressure phase of polyethylene, including hexagonal packing, expansion of the *a* and *b* lattice parameters, a high proportion of *gauche* defects and rapid sliding of the chains parallel to the chain axis [1,3,5,15,8]. It is only observed in the finite and jogged chain models, because the chains in the infinite-chain models are unable to contract due to the constraints imposed by the periodic boundary conditions. This highlights the importance of chain-ends in the formation of mobile phases.

The occurrence of the contracted chain mobile phase in the jogged chain model is particularly interesting, firstly because it occurs at ambient pressure, and secondly because this model is physically the most similar to a chain-folded polyethylene crystal. This is partly due to the length of the chain stems, but also because the jogs have a similar effect to chain-folds, in allowing the chain to pass more than once through the crystal. Generally we would expect to apply pressure to form a mobile phase, because otherwise the thermal energy required would lead to melting. However, in the case of the jogged-chain model, it seems likely that the constraint imposed by allowing the chain to pass twice through the simulation box is sufficient to pin the structure together, at least over the narrow temperature window in which we have observed the mobile phase. It would be interesting to continue working with this model at elevated pressures, and this will be the subject of future work.

In addition to the contracted-chain phases, two examples have been shown of an extended-chain rotator phase, a well characterised feature of short *n*-alkanes [31,33]. There are some similarities between the two types of mobile phase, including a close-to-hexagonal chain packing arrangement and an increased chain mobility in the form of chain sliding and rotation. However, there are also significant differences. For example, the extended-chain phases occur at higher densities than the contracted-chain phases, and this leads to a lower chain mobility in the extended-chain case. Also, the molecules in the extended-chain phases rotate as near-rigid rotors, while, in the contracted-chain phases, the rotations of individual 3MS units are relatively uncorrelated.

Table 3
A summary of the mobile phases identified in this simulation study

Model	Pressure (kbar)	*T* (K)	Nature of hexagonal phase
4×6×12 (infinite chain)	5	550	Extended-chain
4×6×C_{24} (finite chain)	5	350	Extended-chain
	5	400–450	Contracted-chain
4×6×C_{102} (jogged chain)	0	440	Contracted-chain
Branched model (20.8 SCB/1000C)	0	300	Intermediate

The basic requirement for the formation of a rotator phase appears to be the provision of extra free volume, while constraining the polymer chains to remain parallel. This normally occurs through a combination of thermal energy and pressure. In the small computer models considered here, an additional constraint is present due to the boundary conditions, which influence the ability of the chains to reorient to a limited extent in all cases. Thus, it is generally possible to create a rotator phase if sufficient free volume is introduced by whatever means—this explains the occurrence of a rotator phase in a highly branched system at room temperature (Fig. 16, Tables 2 and 3).

The lattice parameters predicted for the three models show a reasonable level of agreement with experimental values, but there is clearly room for improvement. The jogged chain model shows qualitative agreement with experiment, but not a quantitative agreement due to the difference in pressure. However, the jogged chain model correctly predicts a jump in lattice parameters on forming the contracted-chain pseudo-hexagonal phase, of approximately the right magnitude, which is necessary to accommodate the wider, conformationally disordered chains. On the other hand, the infinite chain model, while agreeing quite well with the experimental lattice parameters at the lower temperatures, displays a smooth transition to the extended-chain pseudo-hexagonal phase. This contrasting behaviour is characteristic of the two types of phase. In the language of phase transitions, we might label the transition to the extended-chain phase as displacive, while that to the contracted-chain phase is reconstructive.

Overall, the behaviour exhibited by the simulated phases demonstrates that the choices of model and force field were appropriate for this study of mobile phases. Although the experimental cell parameters were not reproduced identically, the major trends of the systems were captured, and useful insights obtained. In the future, we intend to refine our simulations, both by considering more realistic models and by employing more detailed force fields.

5. Conclusions

Three computer models have been considered as possible candidates for simulating the mobile phase of polyethylene. This phase, which is characterised by a high degree of conformational disorder, and translational motion, occurs under conditions of elevated pressure and temperature [1–6]. Each model consists of chains, which are short compared with the typical fold separation in chain-folded polyethylene crystals, and each incorporates a different level of disorder. By a careful choice of system parameters it has been possible to simulate two different kinds of mobile phase, both of which feature pseudo-hexagonal chain packing. The most ordered system consists of straight chain segments, bonded across the simulation box boundaries to create infinite chains. This system forms a rotator phase in which the chains remain substantially in the all-*trans* conformation. A similar phase is found in a system containing finite *n*-alkane chains when simulated at lower temperatures. This phase is referred to as an

extended-chain rotator phase. The phase is characterised by frequent chain rotations on a time scale of 1–10 ps, and rapid sliding of the chains parallel to their axes. The chains rotate as near-rigid entities. Experimentally, such behaviour is typical of the rotator phases of *n*-alkanes [31,33], but not of polyethylene. The other rotator phase simulated is found in the *n*-alkane model at higher temperatures, and also in a novel model containing jog defects, in which each chain passes through the simulation cell twice. The chain-stems in this phase contain a large proportion of *gauche* defects which cause them to become shorter, and to have a greater effective width. For this reason the phase is referred to as a contracted-chain rotator phase. The positions of the defects within each chain, even on the picosecond time scale of this work, are far from static. As a result, the phase also experiences frequent chain rotations and chain sliding, in common with the extended-chain case. However, translational diffusion is more rapid in the contracted-chain phase than in the extended-chain one. The contracted chain phase is also characterised by a discontinuous increase in lattice parameter values on formation, which is necessary to accommodate the increased lateral dimensions of the disordered chain stems. The contracted-chain rotator phase gives a qualitatively close representation of the behaviour expected in the mobile phase of polyethylene. To the best of our knowledge, this is the first reported fully atomistic simulation of a conformationally disordered mobile phase of this type. Work is in hand to extend the simulations in order to achieve more quantitative agreement with experimental results.

Acknowledgements

The authors with to thank the H.H. Wills Physics Department, University of Bristol, and the EPSRC for supporting this project through a PhD studentship, Drs A.E. Terry, J.K. Hobbs and P.J. Barham for helpful discussions about polyethylene, and Profs M.P. Allen and J.H.R. Clarke for advice on computational methods. The assistance of Dr D.R. Binger with computational support is gratefully acknowledged.

References

[1] Geil PH, Anderson FR, Wunderlich B, Arakawa TJ. Morphology of polyethylene crystallized from the melt under pressure. J Polym Sci A 1964;2:3707–20.
[2] Yasuniwa M, Nakafuku C, Takemura T. Melting and crystallization process of polyethylene under high-pressure. Polym J 1973;42:526–33.
[3] Bassett DC, Block S, Piermarini GJ. A high-pressure phase of polyethylene and chain-extended growth. J Appl Phys 1974;45:4146–50.
[4] Yasuniwa M, Enoshita R, Takemura T. X-ray studies of polyethylene under high pressure. Jpn J Appl Phys 1976;15:1421–8.
[5] Yamamoto T, Miyaji H, Asai K. Structure and properties of high pressure phase of polyethylene. Jpn J Appl Phys 1977;16:1891–8.
[6] Hikosaka M, Tsukijima K, Rastogi S, Keller A. Equilibrium triple point pressure and pressure temperature phase-diagram of polyethylene. Polymer 1992;33:2502–7.
[7] Tanaka H, Takemura T. Studies on the high-pressure phases of polyethylene and poly(tetrafluoroethylene) by Raman spectroscopy. Polym J 1980;120:355–61.
[8] Tashiro K, Sasaki S, Kobayashi M. Structural investigation of orthorhombic-to-hexagonal phase transition in polyethylene crystal: the experimental confirmation of the conformationally disordered structure by X-ray diffraction and infrared/Raman spectroscopic measurements. Macromolecules 1996;29:7460–9.
[9] Klein PG, Robertson MB, Driver MAN, Ward IM, Packer KJ. Chain diffusion in polyethylene and *n*-alkane crystals observed by Carbon-13 NMR. Polym Int 1998;47:76–83.
[10] de Langen M, Prins KO. Mobility of polyethylene chains in the orthorhombic and hexagonal phases investigated by NMR. Chem Phys Lett 1999;299:195–200.
[11] Klein PG, Driver MAN. Chain diffusion in ultralong *n*-alkane crystals studied by ^{13}C NMR. Macromolecules 2002;35:6598–612.
[12] Shahin MM, Olley RH, Bassett DC, Maxwell AS, Unwin AP, Ward IM. Morphological changes in pressure annealed polyethylene. J Mater Sci 1996;31:5541–9.
[13] Maxwell AS, Unwin AP, Ward IM. The mechanical behaviour of oriented high-pressure annealed polyethylene. Polymer 1996;37:3283–91.
[14] Keller A, Hikoska M, Rastogi S, Toda A, Barham PJ, Goldbeck-Wood G. An approach to the formation and growth of new phases with application to polymer crystallization effect of finite size, metastability and Ostwald rule of stages. J Mater Sci 1994;29:2579–604.
[15] Hikosaka M, Rastogi S, Keller A, Kawabata H. Investigations on the crystallization of polyethylene under high-pressure—role of mobile phases, lamellar thickening growth, phase-transformations, and morphology. J Macromol Sci 1992;B31:87–131.
[16] Sumpter BG, Noid DW, Wunderlich B. Computer experiments on the internal dynamics of crystalline polyethylene: mechanistic details of conformational disorder. J Chem Phys 1990;93:6875–89.
[17] Liang GL, Noid DW, Sumpter BG, Wunderlich B. Molecular-dynamics simulations of the hexagonal structure of crystals with long methylene sequences. J Polym Sci, Part B: Polym Phys 1993;31:1909–21.
[18] Kreitmeier SN, Liang GL, Noid DW, Wunderlich B. Molecular-dynamics simulation of the temperature-dependence of lattice-parameters of alkane crystals during cooling. J Chem Soc, Faraday Trans 1995;91:2601–8.
[19] McGann MR, Lacks DJ. Chain length effects on the thermodynamic properties of *n*-alkane crystals. J Phys Chem B 1999;103:2796–802.
[20] Oleinik E, Karmilov I, Shenogin S, Kalashnikov A, Mazo M, Balabaev N, Chvalun S. Computer modelling of structure and dynamics of C-50 *n*-paraffin crystal, hexagonal phase of C-50 crystal and ethylene/propylene statistical copolymers. Macromol Symp 1999;146:133–43.
[21] Mavrantza I-E, Prentzas D, Mavrantzas VG, Galiotis C. Detailed atomistic molecular-dynamics simulation of the orthorhombic phase of crystalline polyethylene and alkaline crystals. J Chem Phys 2001;115:3937–50.
[22] Mowry SW, Rutledge GC. Atomistic simulations of the α_c-relaxation in crystalline polyethylene. Macromolecules 2002;35:4539–49.
[23] Phillips TL, Hanna S. A comparison of computer models for the simulation of crystalline polyethylene and the long *n*-alkanes. Polymer, in press, doi:10.1016/j.polymer.2005.09.040.
[24] Gusev AA, Zehnder MM, Suter UW. Molecular modelling of polymers. In: Mattice WL, editor. ACS short courses. Washington, DC, USA: American Chemical Society; 1996.
[25] Martoňák R, Paul W, Binder K. Orthorhombic phase of crystalline polyethylene: a Monte Carlo study. J Chem Phys 1997;106:8918–30.
[26] Yamamoto T. Monte Carlo simulation of the crystal-structure of the rotator phase of *n*-paraffins. J Chem Phys 1985;82:3790–4.
[27] Yamamoto T. Monte Carlo simulation of the crystal structure of the rotator phase of *n*-paraffins. II. Effects of rotation and translation of the rigid molecules. J Chem Phys 1988;89:2356–65.
[28] Fujiwara S, Sato T. Molecular dynamics simulation of structure formation of short chain molecules. J Chem Phys 1997;110:9757–64.
[29] Yamamoto T, Matsumoto S, Hirose M. A Monte Carlo study of the pattern formation during transitions in *n*-alkane crystals. J Chem Phys 2000;112:7627–33.
[30] Sumpter BG, Noid DW, Liang GL, Wunderlich B. Atomistic dynamics of macromolecular crystals. Adv Polym Sci 1994;116:27–72.

[31] Ryckaert JP, McDonald IR, Klein ML. Disorder in the pseudohexagonal rotator phase of *n*-alkanes: Molecular-dynamics calculations for tricosane. Mol Phys 1989;67:957–79.
[32] Russell KE, Wu G, Blake S, Keyding RD. ^{13}C NMR and X-ray diffraction studies of the morphology of alkanes and linear polyethylenes. Polymer 1992;33:951–7.
[33] Sirota EB, King HE, Singer DM, Shao HH. Rotator phases of the normal alkanes: An X-ray scattering study. J Chem Phys 1993;98:5809–24.
[34] Ryckaert JP. On the simulation of plastic crystals of *n*-alkanes with an atomistic model. Physica A 1995;213:50–60.
[35] Bunn CW. The crystal structure of long-chain normal paraffin hydrocarbons. The 'shape' of the CH_2 group. Trans Faraday Soc 1939; 35:482–91.
[36] Smith GD, Yoon DY. Equilibrium and dynamic properties of polymethylene melts from molecular dynamics simulations. I. *n*-tridecane. J Chem Phys 1994;100:649–58.
[37] Smith W, Forester TR. DL-POLY-2.0—a general-purpose parallel molecular-dynamics simulation package. J Mol Graphics 1996;14: 136–41.
[38] Phillips TL, Hanna S. A molecular dynamics study of the effect of ethyl branches on the orthorhombic structure of polyethylene. Polymer, in press, doi:10.1016/j.polymer.2005.09.018.
[39] Berendsen HJC, Postma JPM, van Gunsteren WF, DiNola A, Haak JR. Molecular dynamics with coupling to an external bath. J Chem Phys 1984; 81:3684–90.
[40] Ryckaert JP. Special geometrical constraints in the molecular-dynamics of chain molecules. Mol Phys 1985;55:549–56.
[41] Allen MP, Tildesley DJ. Computer simulation of liquids. Oxford: Oxford Science Publications; 1987.
[42] Doherty DC, Hopfinger AJ. Molecular modeling of polymers: molecular dynamics simulation of the rotator phase of $C_{21}H_{44}$. Phys Rev Let 1994; 72:661–4.
[43] Ryckaert JP, Klein ML. Translational and rotational disorder in solid *n*-alkanes: constant temperature-constant pressure molecular dynamics calculations using infinitely long flexible chains. J Chem Phys 1986;85: 1613–20.
[44] Guillaume F, Doucet J, Sourisseau C, Dianoux AJ. Molecular motions in *n*-nonadecane $C_{19}H_{40}$: an incoherent neutron scattering study. J Chem Phys 1989;91:2555–67.
[45] Guillaume F, Elbaghdadi A, Dianoux AJ. Dynamics of alkyl-type chains in crystals. Phys Scr 1993;T49B:691–8.
[46] MacDowell LG, Guillaume F, Ryckaert JP, Girard P, Rodriguez V, Dianoux AJ. Rotational molecular dynamics in the R-I phase of *n*-nonadecane. Physica B 1997;234:106–8.
[47] Boyd RH. Relaxation processes in crystalline polymers—experimental behavior—a review. Polymer 1985;26:323–47.
[48] Boyd RH. Relaxation processes in crystalline polymers—molecular interpretation—a review. Polymer 1985;26:1123–33.
[49] Zhang F. Motion of twist defects in crystalline polyethylene: a molecular-dynamics study. Phys Rev B 1999;59:792–6.
[50] Dorset DL, Hu HL, Jager J. Continuous diffuse-scattering from polymethylene chains—an electron diffraction study of crystalline disorder. Acta Crystallogr Sect A 1991;47:543–9.
[51] Busing WR. X-ray diffraction study of disorder in Allied Spectra-1000 polyethylene fibres. Macromolecules 1990;23:4608–10.